Frontiers of Information Technology & Electronic Engineering
www.jzus.zju.edu.cn; engineering.cae.cn; www.springerlink.com
ISSN 2095-9184 (print); ISSN 2095-9230 (online)
E-mail: jzus@zju.edu.cn

Sensor-guided gait-synchronization lower-extremity-exoskeleton for potential application on unilateral knee-injured people*

Donghai WANG[1,2]

[1]*State Key Laboratory of Digital Manufacturing Equipment and Technology, Huazhong University of Science and Technology, Wuhan 430074, China*
[2]*Guangdong Sygole Intelligent Technology Co., Ltd., Dongguan 523808, China*
E-mail: donghaiwang@hust.edu.cn

Received Sept. 9, 2020; Revision accepted Oct. 8, 2021; Crosschecked June 1, 2022

Abstract: This paper presents a sensor-guided gait-synchronization system to help potential unilateral knee-injured people walk normally with a weight-supported lower-extremity-exoskeleton (LEE). This relieves the body weight loading on the knee-injured leg and synchronizes its motion with that of the healthy leg during the swing phase of walking. The sensor-guided gait-synchronization system is integrated with a body sensor network designed to sense the motion/gait of the healthy leg. Guided by the measured joint-angle trajectories, the motorized hip joint lifts the links during walking and synchronizes the knee-injured gait with the healthy gait by a half-cycle delay. The effectiveness of the LEE is illustrated experimentally. We compare the measured joint-angle trajectories between the healthy and knee-injured legs, the simulated knee forces, and the human-exoskeleton interaction forces. The results indicate that the motorized hip-controlled LEE can synchronize the motion/gait of the combined body-weight-supported LEE and injured leg with that of the healthy leg.

Key words: Sensor-guided; Lower-extremity-exoskeleton; Body sensor network; Gait synchronization; Weight-support
https://doi.org/10.1631/FITEE.2000465 **CLC number:** TP242.6

1 Introduction

Single-sided leg injuries such as unilateral anterior cruciate ligament (ACL) injuries commonly happen in sports (like football, basketball, and gymnastics) and daily activities (Hootman et al., 2007; Brophy et al., 2010; Gupta et al., 2016). The postoperative recovery is a long process, during which patients have to stay on crutches to support their body weight (BW) with their upper limbs when an injured knee is in the stance phase during walking. Single-joint exoskeletons for walking assistance in hip, knee, and ankle joints provide typical examples of mechanical assistance. Kang et al. (2020) presented a powered robotic hip exoskeleton to provide power assistance along the sagittal plane, and a sensor fusion based neural network model was developed to estimate the gait phase in real time and adapt to dynamic speeds. Liu XH and Wang (2020) designed a unilateral knee exoskeleton to supply appropriate assistive torque based on real-time accurate recognition of current gait mode and specific assistive control strategies. Wang TM et al. (2020) presented an untethered cable-driven ankle exoskeleton that can achieve plantarflexion-dorsiflexion bidirectional motion bilaterally using a pair of single motors, and the reduced muscle activity verifies the positive assistance effect. The above joint exoskeletons revealed the excellent performance in joint walking assistance, and the convincing experimental results indicated the potential of an exoskeleton for assistance with single-sided leg injuries.

* Project supported by the National Natural Science Foundation of China (No. 51705167) and the Dongguan Introduction Program of Leading Innovative and Entrepreneurial Talents
ORCID: Donghai WANG, https://orcid.org/0000-0002-4523-8480
© Zhejiang University Press 2022

This paper focuses only on the potential unilateral knee joint injuries. However, the transfer of BW to the ground relies on the whole lower limbs including the hip, knee, and ankle joints, and the lower-extremity-exoskeletons (LEEs) are considered rather than the single-joint exoskeleton. LEEs capable of supporting BW and adapting to human joint/gait variations provide a possible means to free the hand and rehabilitate the biological joints to prevent musculoskeletal decline. For example, He et al. (2019) proposed a novel intelligent autonomous LEE with 10 actuated degrees of freedom, and the robot was validated to have the ability of self-balance during bipedal walking and maintaining balance in aiding walking without extra support. Existing rehabilitation LEEs can be broadly classified into two categories based on actuation: active and passive. Active LEEs train patients by actuating their passive joints using offline gait data or pre-measured trajectories (Dollar and Herr, 2008); typical examples include the hydraulic LEE (Kim et al., 2017), the hybrid assistive limb (HAL) (Tsukahara et al., 2015), and walking exoskeleton (Zhang T et al., 2018). Traditionally, active rehabilitation LEEs are designed to provide motion assistance to completely disabled patients such as paraplegics (Chen B et al., 2019) and are recently developed for patients with unilateral lower limb movement disorders (Zhang C et al., 2016). Lithium batteries have been widely used in these active LEEs to manipulate passive legs. Unfortunately, these batteries can last only several hours. As a result, LEEs with bulky weight, which not only hinder dexterous movement of the human leg but also consume power, are not widely used in outdoor training. More recently, a passive LEE (Wang DH et al., 2016) where compliant mechanisms are incorporated in the design to adapt to human biological joints has been developed to reduce knee load for people (such as senior citizens) who suffer from knee pain during walking. Without the need for large-capacity batteries to drive powered actuators, the passive BW-supported LEE (P-BWS-LEE) enjoys some advantages including light weight, low cost, and safety in physical interaction between human and exoskeleton. Built upon the attractive features offered by the P-BWS-LEE (Wang DH et al., 2016), a low-cost unilateral LEE has been developed for unilateral knee-injured patients whose other body parts (including the hip joint) are intact and capable of maintaining body balance in the process of locomotion. Although only healthy subjects are included in this paper, the experimental results in Section 3 show the positive potential application of a unilateral LEE on the unilateral knee-injured patients. So, here the potential unilateral knee-injured patients are assumed to be reasonably applicable subjects. The primary functions of the unilateral LEE are to relieve loads on the potential injured knee during the stance phase, measure gait motion of the healthy leg in real time, and synchronize the gait of the knee-injured leg with that of the healthy leg.

Human gait trajectories, which are dependent on BW and are highly influenced by individual walking habits and speeds (Malcolm et al., 2018), vary from one to another. Thus, real-time gait sensing is essential to characterize the gait of the healthy leg, where plantar force sensors and inertial sensors are commonly used. Plantar force sensors are typically embedded in shoes, e.g., smart insoles (Lin et al., 2016) and sensor shoes (Li GY et al., 2016). Shoe-embedded force sensors, however, are susceptible to wear and tear because of the high load and high frequency of foot forces during walking, and the data are extremely sensitive to small amounts of unevenness in the ground. Because of light weight, small size, and being force free (Liu Q et al., 2019), inertial sensors (like accelerometers or gyroscopes) are increasingly used in body sensor networks (BSNs) (Uddin et al., 2020), stance-phase detection systems (Wang ZL et al., 2015), and data-driven methods to improve human-machine coordination. Fusing the above two types of sensors, Wang TM et al. (2020) designed a creative gait detection system based on a foot pressure sensor and an inertial measurement unit (IMU). It can identify human gait states accurately and efficiently. Long et al. (2018) proposed an LEE that obtained physical human-robot interaction torque from torque sensors perceiving intended human motion, and estimated human gait trajectories to implement corresponding actions quickly and accurately. Among these data-driven methods (including a human-cooperative adaptive fuzzy control strategy with virtual tunnels (Li ZJ et al., 2020), a gait-event-based synchronization method with adaptive oscillators (Chen G et al., 2017), and synchronization-based control design using neural

oscillators (Mizukami et al., 2018)), trained artificial neural networks (ANNs) are computationally efficient (Barton et al., 2007). They exhibit excellent learning capability in a noisy environment with high interpolation accuracy (Lugade et al., 2014). Thus, a measurement-based ANN could offer a viable easy-to-implement approach in real-time applications. An ANN that determines the gait phase from a low-cost BSN could be designed to eliminate commonly used shoe-embedded sensors that are susceptible to wear and tear as described. However, the potential of low-cost IMU for effective gait synchronization is underexploited because the relationships between the gait phases and the measured joint angles of the lower extremity are not well understood.

To address the issues including relieving loads on the injured knee during the stance phase and synchronizing the gait of the knee-injured leg with that of the healthy leg, we propose the design concept of a unilateral LEE to help one-side-knee-injured people walk normally. This paper presents a lightweight unilateral LEE with a sensor-guided gait-synchronization system, which reduces the load on the injured knee by supporting the patient's BW during stance and allows the healthy leg to maintain control of the overall balance. The sensor-guided gait-synchronization system obtains patient-specific gait/motion data of the healthy leg in real time and synchronizes the combined unilateral LEE/knee-injured leg with the healthy leg to prevent imbalance during walking. The proposed sensor-guided gait-synchronization LEE takes advantages of both active and passive LEEs. It relieves the load on the injured leg by transferring human BW directly to the ground during the stance phases while synchronizing its walking gait (both the joint angles and gait cycles) with that of the healthy leg (gait, posture, and speed); the latter prevents hindering his/her natural movement in the subsequent swing phases.

2 Unilateral LEE for knee-injured people

Normal human gait can be broadly classified into five sequential phases: IC (initial contact), MS (mid stance), TS (terminal stance), PS (pre-swing), and SP (swing phase). During the stance phases (IC, MS, TS), the human body is rotated forward about the supporting foot (by momentum like an inverted pendulum); no external actuation is needed. Fig. 1 illustrates the unilateral LEE designed to relieve the BW on the injured (assumed left) knee in the stance phases, offer an external torque to overcome the dynamic/gravitational forces of the combined LEE/leg, and synchronize with the healthy leg in the swing phases (PS, SP). The hip is at the top of the cascaded structure

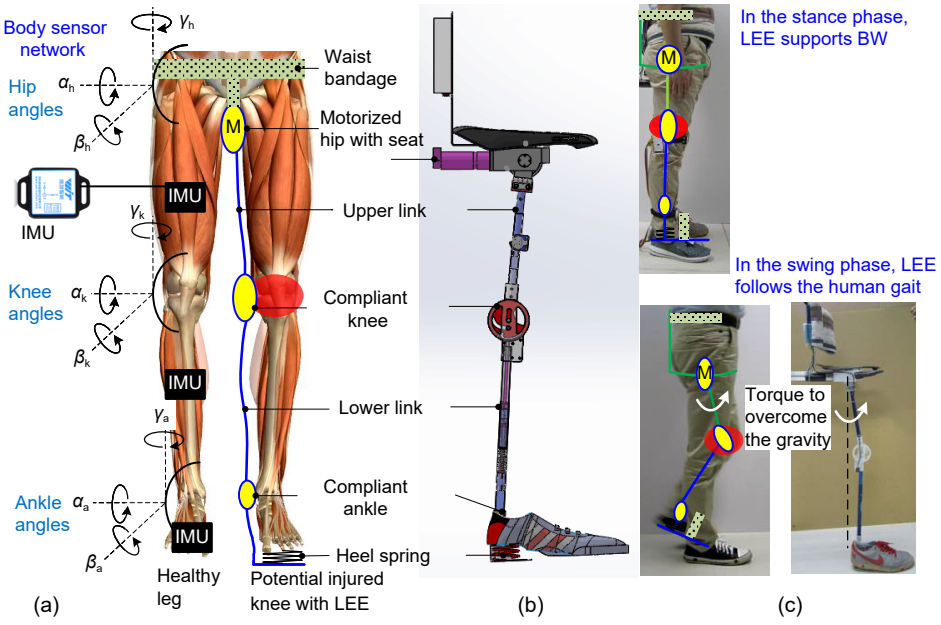

Fig. 1 Unilateral LEE design concept: (a) overall schematics; (b) BWS-LEE with a motorized hip; (c) stance/swing phase

of the lower limb, and the LEE knee joint swings forward by inertia like a swing and does not need driving torque as a hip joint. Considering the tradeoff between LEE's light weight and gait synchronization, the LEE is designed with an active hip joint and a passive knee joint. Belt-fastened between the waist and shoe, the knee-injured patient rides on the unilateral LEE that consists of two major subsystems during walking: a BSN to distinguish the gait of the healthy leg, and a BWS-LEE (Fig. 1b) with the injured leg to bear the BW. At present, the main application scenarios in which the BWS-LEE is used are walking on the ground, not stairs.

An effective method to determine gait phases is to measure plantar forces using shoe-embedded force sensors that, however, are susceptible to wear and tear as mentioned. To eliminate the need to rely on shoe-embedded sensors, the BSN determines the gait phase from the motion measurements (α_j, β_j, γ_j) (j=h, k, a) of the healthy joints, where the subscripts h, k, and a refer to the hip, knee, and ankle joints, respectively. The trunk is assumed to be vertical during the whole gait, and the angle measurements (α_j, β_j, γ_j) of the joints are not related to the trunk. Together with an offline trained ANN (Fig. 2), the BSN provides a reference to the unilateral LEE for synchronizing the knee-injured gait. As an illustration (Fig. 1), three IMUs are used to measure the joint angles (α_j, β_j, γ_j) of the healthy leg. For an injured knee capable of flexion, only a single actuator is incorporated for self-compensating for the weight of the added mechanism. Built upon the P-BWS-LEE design concept (Wang DH et al., 2016), compliances are incorporated in the mechanical ankle and knee to accommodate the human joint variations. The stiffness of the compliant ankle joint is configured by considering the LEE to support 20% of the body weight, and the stiffness of the compliant knee joint is configured based on human gait phases with dual-snap-fit mechanism design. A higher stiffness in compliant mechanisms would reduce more load for the knee. However, it would also affect human movement. A practical stiffness design in compliant mechanisms must trade between two requirements (BW support and compliance in joint coupling). A motorized hip joint and its associated control system are designed for the unilateral LEE as shown in Fig. 2. The offline ANN training and the control system implementation for the injured knee are detailed in Sections 2.1 and 2.2 respectively.

2.1 ANN and gait synchronization algorithm

Based on the measured joint angles (α_j, β_j, γ_j) of the healthy leg, the ANN algorithm generates the reference trajectory to control the motorized hip joint.

2.1.1 Offline training of ANN

Fig. 3 shows the BSN setup for offline training of the ANN that exhibits excellent learning capability

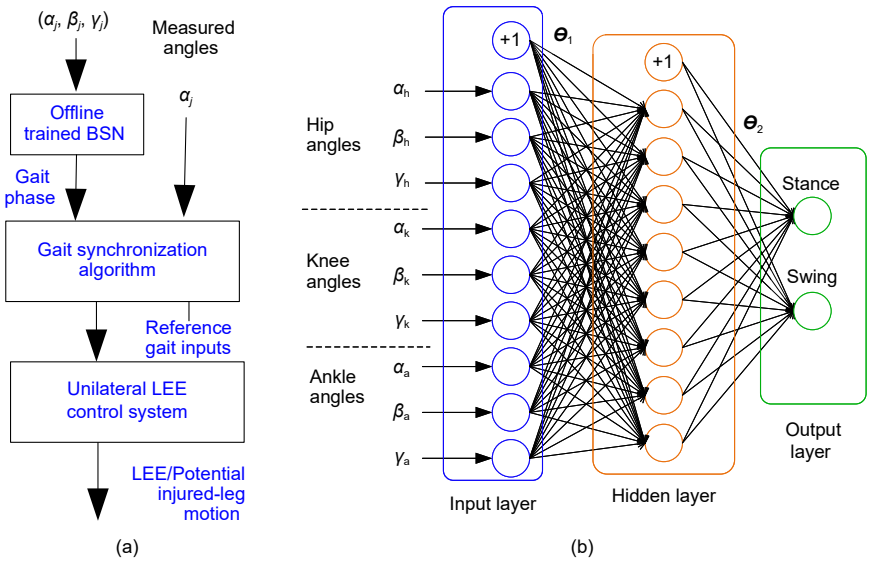

Fig. 2 Sensor-guided gait synchronization: (a) flowchart illustrating the unilateral LEE control strategy; (b) ANN training

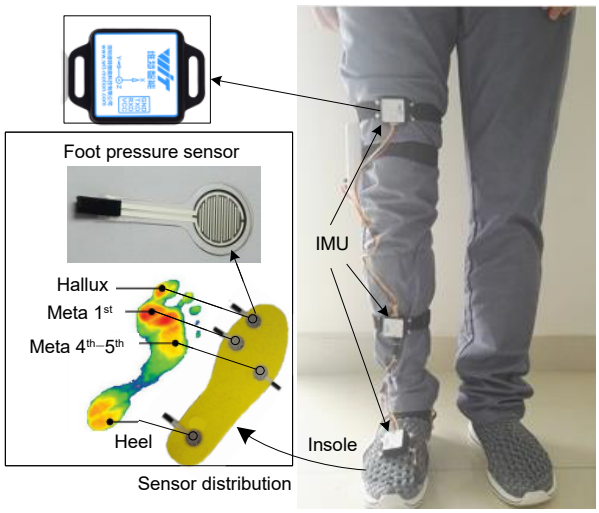

Fig. 3 BSN setup for offline ANN training

in a noisy environment with high interpolation accuracy. The input angles are measured by the IMUs, and the specific phase in a gait cycle is determined from the plantar forces. As illustrated in Fig. 2b, each sample consists of nine inputs and two outputs. The training data are preprocessed and normalized to improve the convergence rate and quality. Once trained, the measurement-based ANN offers a computationally efficient approach.

As shown in Fig. 3, four binary foot-force sensors θ_i (i=1 refers to the sensor attached to the heel; i=2 refers to the sensor attached to the 4th–5th toes; i=3 refers to the sensor attached to the 1st toe; i=4 refers to the sensor attached to the hallux) are employed to determine the specific phase in a gait cycle from the plantar forces (Yu et al., 2010) (but are not required in actual operation of the unilateral LEE). The i^{th} sensor outputs a binary number as defined in Eq. (1) from the measured force f_i:

$$\theta_i = \begin{cases} 1, f_i > \xi\,(\text{pressed}), \\ 0, 0 < f_i \leqslant \xi\,(\text{not pressed}), \end{cases} \tag{1}$$

where $\xi=\lambda+\eta$ with λ being a measured value without load to account for environmental effects (such as zero or small temperature shift and workplace noise) and η providing sensitivity regulation. Smaller η values result in higher detection sensitivity (to noise).

The ANN training (Fig. 2b) consists of an input layer of nine joint angles (α_j, β_j, γ_j), a hidden layer of eight nodes, and an output layer of two nodes. The stance phase is (1, 0) and the swing phase is (0, 1).

$$\text{Stance}\,(\text{ST}) = \begin{cases} \theta_1 \times \overline{\theta}_2 \times \overline{\theta}_3 \times \overline{\theta}_4\ (\text{IC}), \\ \theta_1 \times \theta_2\ (\text{MS}), \\ \overline{\theta}_1 \times \theta_3\ (\text{TS}), \end{cases} \tag{2a}$$

$$\text{Swing}\,(\text{SW}) = \begin{cases} \overline{\theta}_1 \times \overline{\theta}_2 \times \overline{\theta}_3 \times \theta_4\ (\text{PS}), \\ \overline{\theta}_1 \times \overline{\theta}_2 \times \overline{\theta}_3 \times \overline{\theta}_4\ (\text{SP}), \end{cases} \tag{2b}$$

where $\overline{\theta}_i$ represents the NOT operation in the Boolean algebra. To illustrate the offline training, the phase durations of a gait cycle are experimentally obtained from 12 adults. The five sequential phases (Eqs. (2a) and (2b)) based on the four shoe-embedded force sensor outputs defined in Eq. (1) with η=5 N (Yu et al., 2010) are listed in Table 1, where the average (Ave), standard deviation (SD), maximum (Max), and minimum (Min) values are summarized. The relative portions of the stance and swing phases are approximately 63% and 37% of a gait cycle respectively, and can vary widely.

Table 1 Individual phase duration

Subject	Cycle	Ratio of phase duration to a gait cycle (%)						
	(s)	IC	MS	TS	PS	SP	Stance	Swing
1	1.4	1.6	34.6	29.8	2.2	31.8	66.0	34.0
2	1.2	2.4	35.0	27.3	1.9	33.4	64.7	35.3
3	1.2	3.6	38.8	23.2	2.0	32.4	65.6	34.4
4	1.4	4.5	43.3	14.1	3.6	34.5	61.9	38.1
5	1.4	2.4	38.5	18.4	2.6	38.1	59.3	40.7
6	1.5	5.8	38.9	19.7	1.8	33.8	64.4	35.6
7	1.2	2.5	44.5	19.1	1.1	32.8	66.1	33.9
8	1.3	2.9	36.4	23.2	3.3	34.2	62.5	37.5
9	1.5	5.0	37.5	21.1	2.3	34.1	63.6	36.4
10	1.4	2.1	37.2	21.6	2.1	37.0	60.9	39.1
11	1.3	1.5	29.3	29.5	1.1	38.6	60.3	39.7
12	1.4	1.4	34.4	22.1	6.0	36.1	57.9	42.1
Ave	1.35	2.98	37.37	22.43	2.50	34.73	62.77	37.23
SD	0.11	1.45	4.04	4.63	1.33	2.23	2.74	2.74
Max	1.50	5.80	44.50	29.80	6.00	38.60	66.10	42.10
Min	1.20	1.40	29.30	14.10	1.10	31.80	57.90	33.90

The ANN model (Fig. 2b) is trained using the gait data of three healthy subjects (denoted as A, F, and H) to distinguish the stance and swing phases by the three joint angle sensors. Each input-output pair for training the ANN parameters ($\boldsymbol{\theta}_1$, $\boldsymbol{\theta}_2$) consists of the joint angles and their corresponding gait phases (Eqs. (2a) and (2b)) of the healthy leg. Preliminary

trials suggest that the cost function converges to less than 0.5 within 500 iterations, small enough for this application; for simplicity, a maximum number of 500 iterations is set as a convergence criterion in this study. The program, coded by Matlab using some of its advanced optimizer functions, is computed on a PC (with Intel Core i5-3317U CPU). The results of the ANN offline training are summarized in Table 2, where the training and testing data in every column are for the same subject for patient-specific applications.

For each subject, the gait phase (determined from foot-force sensor data) and the corresponding joint angles (measured using three IMUs) are obtained for a small number (10) and a large number (more than 45) of steps to separately train the ANN. The trained network is then tested using data with a similar number of steps to verify the ANN. The accuracy of the ANN is represented by the percentage of the correct gait phase result detected by the ANN to that detected by the foot pressure sensors, where the results detected by the foot pressure sensors are regarded to be correct.

The trained ANN is evaluated against the gait phases detected by the foot sensors (Table 2). For each subject, the larger number of steps increases the training accuracy (in the order of 1%) but needs significantly more time in training (in the order of 400%) as shown in Table 2. Overall, the trained ANN has an accuracy of approximately 97% (trained with either a small or large number of steps), suggesting that the small number of 10 is sufficient for ANN training in practice.

2.1.2 Gait synchronization algorithm

As shown in Fig. 2a, the gait synchronization algorithm generates the reference trajectory based on the gait phase detected by the ANN and measured joint angles α_j in the sagittal plane. A typical set of measured trajectories is depicted in Fig. 4. Figs. 4a and 4b show the knee, ankle, and hip angles (α_k, α_a, α_h) experimentally measured in the sagittal plane over seven gait cycles during walking at a speed of 1.57 m/s. Fig. 4b shows the gait phase transitions (between SW and ST) detected by the ANN.

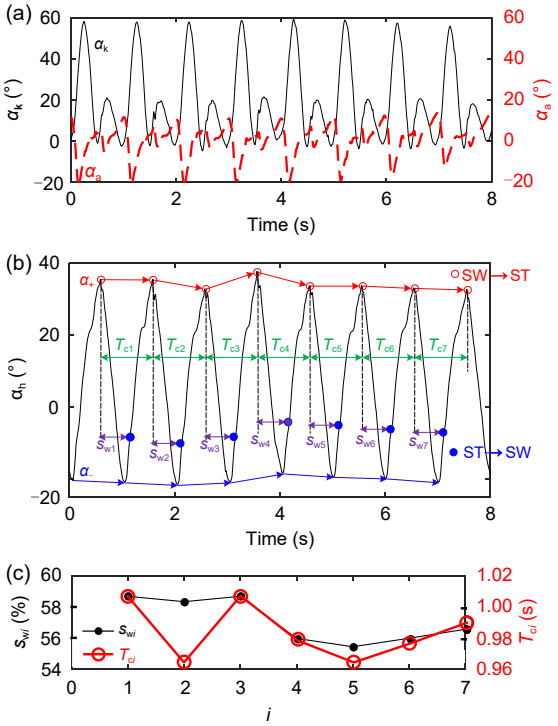

Fig. 4 Joint trajectories of human lower legs in the sagittal plane: (a) knee and ankle angles; (b) hip angle; (c) parameter variations

(SW→ST) transition: red open-circles; (ST→SW) transition: blue filled-circles; percentage of stance, s_{wi}: time between the adjacent (SW→ST) and (ST→SW) over the period T_{ci} in each cycle; (α_+, α_-) are the (maximum, minimum) values of the i^{th} hip joint angle with a period of T_{ci}. References to color refer to the online version of this figure

As shown in Fig. 4c, period T_{ci} and s_{wi} vary somewhat, indicating that the motorized hip must be

Table 2 Results of ANN in comfortable gait

Subject	Training time (s)	Number of training steps	Number of training samples	Number of testing steps	Number of testing samples	Accuracy (%)
A	12.69	10	932	10	951	96.53
A	77.88	58	5318	59	5478	97.28
F	14.92	10	891	10	899	96.33
F	76.77	77	6657	55	4649	97.03
H	11.65	10	710	10	693	96.39
H	43.23	47	3313	47	3244	97.66

synchronized with the healthy leg. The knee and ankle joints repetitively fluctuate between α_k (60° and 0°) and α_a (15° and −20°), respectively.

Fig. 5a illustrates the steps to synchronize the gait of the knee-injured user (the 1st row where the unilateral LEE is on the left leg with an injured knee). The (black, pink) bars represent the (stance, swing) phases in the 2nd row (LEE and injured leg) and 3rd row (healthy leg). The (hip, knee, and ankle) joint angles of the healthy leg (green line in the 3rd row) are measured and saved in real time, and the joint-angle measurements provide the inputs to the ANN to determine the gait phase. The gait synchronization algorithm scans for the swing-motion signal of the healthy leg at the end of each gait cycle. Once the PS motion of the healthy leg is detected, the motorized hip joint is initialized. Since the knee-injured leg requires no external torque during the stance phase, the motorized unilateral LEE follows the healthy leg after a $T_c/2$ (or half a gait cycle) time delay. Gait synchronization is achieved as the trajectories of the motorized hip are updated according to the healthy leg with half a gait cycle time delay, although it cannot be defined strictly as real-time tracking.

Fig. 5b shows a typical hip angle trajectory of a healthy leg in the sagittal plane for a gait period T_c during walking, where the shaded envelop indicates the variation within one standard deviation; s denotes the percentage of the stance phase in a gait cycle. As shown in Fig. 5b, the hip angle decreases monotonously from $\alpha_+=\alpha_h$ (s=0) to its minimum as the body is brought forward by the swing momentum in the 1st half of the gait cycle. While the healthy leg still supports the BW, the hip joint extends till $\alpha_-=\alpha_h$ ($s=s_w$), where s_w is the percentage of stance defined in Figs. 4b and 5b. Finally, the hip joint extends and returns to α_+ during swing to prepare for the next stance. For smooth operation, the measured data within a gait cycle T_c are curve fitted to obtain a continuous hip joint trajectory α_h characterized by the four parameters (α_+, α_-, s_w, T_c):

$$\alpha_h(t)=\begin{cases}(\alpha_+-\alpha_-)(a_3t^3+a_2t^2+a_1t+a_0)+\alpha_-, \\ \quad 0\leqslant t\leqslant s_wT_c, \\ (\alpha_+-\alpha_-)(b_3t^3+b_2t^2+b_1t+b_0)+\alpha_-, \\ \quad s_wT_c<t\leqslant T_c.\end{cases} \tag{3}$$

The coefficients, a_0–a_3 and b_0–b_3 in Eq. (3), are determined using least-squares polynomial fitting to generate the reference trajectory α_h ($s_wT_c<t\leqslant T_c$) to drive the motorized hip after $T_c/2$ delay.

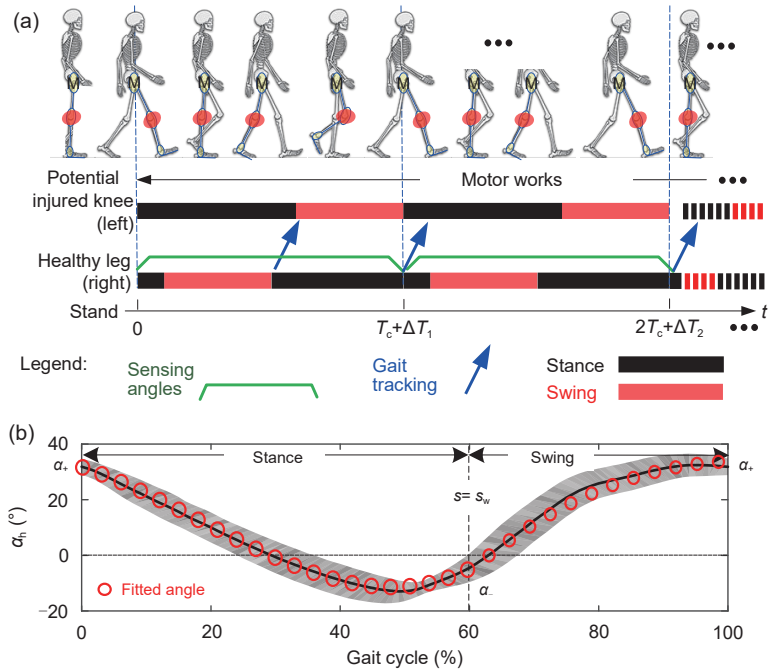

Fig. 5 Gait synchronization: (a) illustration of step timing; (b) a typical curve-fit hip joint trajectory from measurements

References to color refer to the online version of this figure

2.2 Unilateral LEE with motorized hip joint for a potential injured knee

Fig. 6 shows the computer aided design (CAD) and control strategy of the motorized hip joint. The actuating system, which consists of a single degree-of-freedom (DOF) motor with a bevel gear mechanism (Fig. 6a) to generate the motor torque required to swing the combined LEE/leg, is designed to be compactly housed under the seat (Fig. 1b). As illustrated in Fig. 6b, the BSN samples the joint data (α_+, α_-, s_w, T_c) of the healthy leg and these are fed back to the system controller through an inter-integrated circuit (I^2C) protocol. The curve-fit coefficients (b_i, i=0, 1, 2, 3) in Eq. (3) are obtained in each cycle through Bluetooth. Measured by an encoder through universal synchronous asynchronous receiver and transmitter (USART), the motorized hip joint is controlled in two modes:

1. Stance phase: No motorized hip torque ($\tau_1 \approx 0$) is required but the LEE is designed to transfer the BW through its ground contact, thus relieving the load on the injured knee.

2. Swing phase: The motorized hip torque τ_1 is designed to compensate for the dynamic and gravitational effects, and to synchronize the combined injured leg and LEE with the healthy leg using the reference trajectory from the BSN.

Fig. 7 defines the joint parameters of the unilateral LEE and knee-injured leg for analyzing the kinematics and dynamics during the swing phase. The offset d_h between the human and mechanical hip joints can be accounted for by an inverse kinematics that solves for the exoskeleton hip flexion angle θ_h for a specified human hip angle α_h in the sagittal plane (Fig. 7a):

$$\theta_h = \alpha_h + \arcsin\left(\frac{d_h}{l_1}\sin\alpha_h\right). \tag{4}$$

Fig. 7b shows a two-link dynamic model for analyzing the hip torque τ_1 and knee torque τ_2 of the knee-injured leg, where φ_1 and φ_2 are the hip and knee joint angles respectively, f is the ground reaction, and τ_f is the (experimentally calibrated) friction torque. For simplicity, subscripts 1 and 2 respectively refer to parameters of the upper and lower links of the combined human/mechanical mass m, moment-of-inertia I, link length l, and centroid d. Using the Lagrangian formulation, the combined dynamics of the unilateral LEE and knee-injured leg joint is given in Eq. (5), from which the motorized hip torque τ_1 (and thus power P=$|\tau_1\varphi_1|$) can be computed:

$$\frac{1}{m_2 l_2^2}\tau_1 = \boldsymbol{H}\begin{bmatrix}-\ddot{\varphi}_1\\ -\ddot{\varphi}_2\end{bmatrix} + \boldsymbol{C}_o\begin{bmatrix}\dot{\varphi}_1^2\\ \dot{\varphi}_2^2\end{bmatrix} + \frac{g}{l_2}G - \frac{f}{m_2 l_2}F - \tau_f, \tag{5}$$

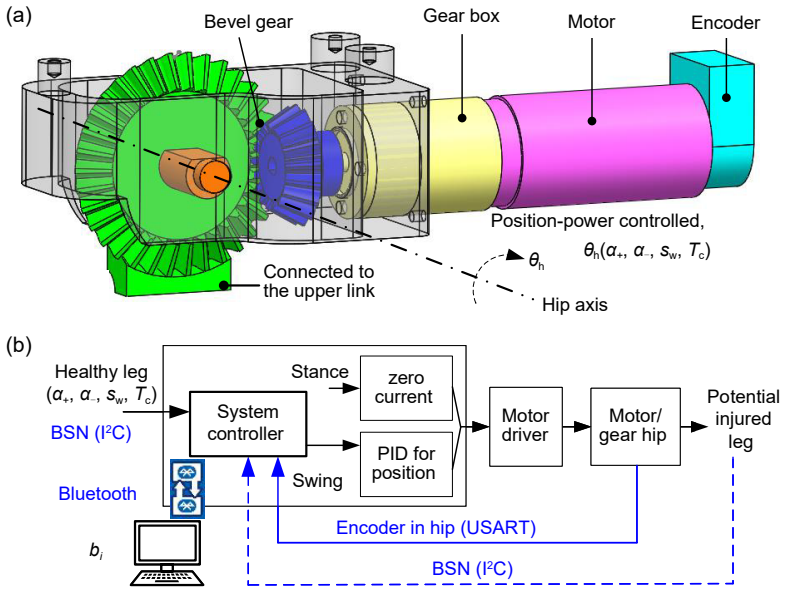

Fig. 6 Unilateral LEE design: (a) motorized hip; (b) control system

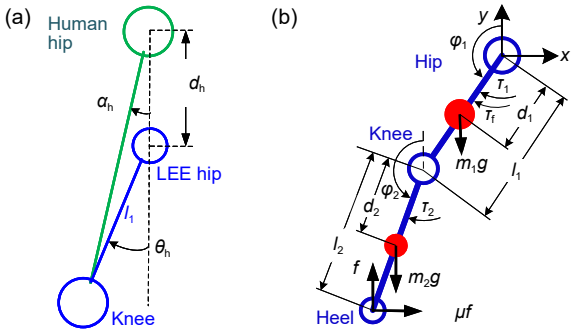

Fig. 7 Parameters used in analysis: (a) kinematics; (b) dynamics

where

$$\boldsymbol{H} = \begin{bmatrix} J_1 + MD_1^2 + L^2 & LD_2C_{12} \end{bmatrix}, \tag{6a}$$

$$\boldsymbol{C}_o = LD_2\begin{bmatrix} 0 & -S_{12} \end{bmatrix}, \tag{6b}$$

$$G = \left(MD_1 + L\right)S_{\varphi 1}, \tag{6c}$$

$$F = S_{\varphi 1} + \mu_m\left|\frac{\theta_h}{\max\left(\theta_h\right)}\right|C_{\varphi 1}\mathrm{sgn}\left(\frac{\mathrm{d}}{\mathrm{d}t}\left|\pi - \varphi_1\right|\right), \tag{6d}$$

where $M=m_1/m_2$ and $L=l_1/l_2$.

In Eq. (5), the dimensionless matrices ($\boldsymbol{H}$, $\boldsymbol{C}_o$) and scalars (G, F) are associated with the inertia, centrifugal, gravity, and ground reaction, and are given in Eqs. (6a)–(6d), where the parameters are normalized to m_2 and l_2 in Eqs. (7a)–(7d) to facilitate designs:

$$\frac{M}{m_1/m_2} = 1, \tag{7a}$$

$$\frac{L}{l_1/l_2} = 1, \tag{7b}$$

$$\frac{J_i}{I_i/\left(m_2l_2^2\right)} = 1, \tag{7c}$$

$$\frac{D_i}{d_i/l_2} = 1. \tag{7d}$$

In Eqs. (6a)–(6d), $C_{12}=\cos(\varphi_1-\varphi_2)$, $S_{12}=\sin(\varphi_1-\varphi_2)$, $S_{\varphi 1}=\sin\varphi_1$, and $C_{\varphi 1}=\cos\varphi_1$ for simplicity; μ_m is the maximum value of the friction coefficient occurring at the LEE motion limits.

3 Results and discussion

The method to synchronize the LEE with the healthy gait is experimentally investigated on a prototype unilateral LEE as shown in Fig. 8, and the parametric data and specifications are summarized in Table 3. Three configurations are compared: No LEE (C1), P-BWS-LEE (C2), and unilateral LEE (C3), where C1 serves as a basis for evaluation. Three sets of results are organized as follows:

1. Prototype unilateral LEE and its dynamic responses are discussed in Section 3.1.

2. Effect of P-BWS-LEE on the internal knee forces is discussed in Section 3.2.

3. It is desirable that LEE has negligible effects on the walking rhythm, speed, and stability. The similarity between two trajectories (with/without gait synchronization) is used as the performance criterion for

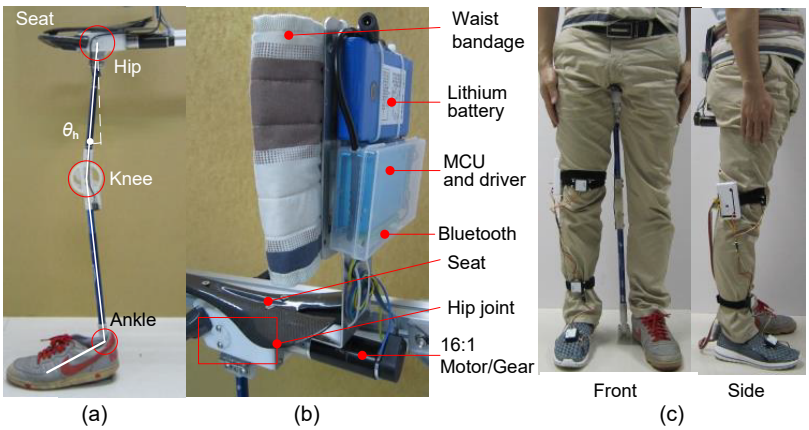

Fig. 8 Experimental prototype: (a) proposed LEE; (b) hip joint actuator and control system; (c) front and side views of a person wearing LEE

Table 3 Specifications of the unilateral LEE

Device	Model	Specification
MCU	STM32F103	72 MHz, 3 USART, 2 I^2C, 37 I/O
Bluetooth	HC-08	80 m, 1 Mb/s, 4 dBm, 31.6 mA
Motor	RM35	24 V, 90 W, 2 N·m, 388 r/min, Φ35×131 mm
Driver	RMDS-107	1–25 000 mA, 1–32 767 r/min
Encoder	REP	500 wires, quadruple, ABZ
Battery	XC-7S26	24 V, 2.6 A·h, maximum current 8 A
IMU	JY901	±180°, resolution: 0.1°, 120 Hz, I^2C
Foot sensor	IMS-C20	80 kg (single-point sensor), resolution: ±2.5% full scale

LEE				
Part (i)	d_i (m)	l_i (m)	m_i (kg)	I_i (kg·m^2)
Upper link + knee (1)	0.288	0.304	0.226	6.8e−04
Lower link + ankle (2)	0.357	0.485	0.286	7.2e−03
μ_m=0.31, d_h=0.15 m, total mass=2.08 kg				

quantitative evaluation using the dynamic time warping (DTW) method (outlined in Appendix). Results comparing C1, C2, and C3 are discussed in Section 3.3.

3.1 Experimental prototype unilateral LEE

The motorized hip joint is driven by a direct current (DC) motor through a 16:1 gear-box and 2:1 bevel-gear mechanism, and is position-controlled by a microcontroller unit (MCU, STM32F103). Fig. 8c shows the front and side views of LEE worn on the left leg of subject A, and the three joint angle sensors (IMUs) worn on the right leg. The total mass of the unilateral LEE (including the battery, motor, seat, and related accessories) is 2.08 kg, which is less than 3.3% of subject A's weight (63.5 kg) and has the large advantage of light weight compared with a traditional exoskeleton (9.2 kg, Zhang T et al., 2018). During walking in practice, the MCU measures the gait data of IMUs in real time, and communicates with the computer through Bluetooth to fit the gait data for the curve-fit coefficients (b_i, i=0, 1, 2, 3). The offline trained ANN parameters ($\boldsymbol{\Theta}_1$, $\boldsymbol{\Theta}_2$) are pre-stored in the MCU, and the real-time gait phases (stance phase and swing phase) are computed by the MCU. The MCU controls the motor by the motor driver with the curve-fit coefficients (b_i, i=0, 1, 2, 3). Zero-current control mode and proportional-integral-differential (PID) control mode are implemented in the stance phase and swing phase, respectively.

The dynamic responses of the closed-loop motorized hip system are experimentally determined (Fig. 9). The seat is mounted on a horizontal aluminum alloy rack with the upper link vertically downward. The friction torque τ_f of the motorized hip is estimated by means of an ATI high-precision force sensor (ATI NANO17), through which the upper link is gradually pulled with zero-input current. From the product of the measured pulling force and moment arm (Figs. 9a and 9b), the maximum friction torque τ_f is experimentally found to be 0.06 N·m, which is 0.15% of the maximum hip torque (40 N·m) in normal gait (Wang DH et al., 2016). The dynamic responses of the closed-loop system are summarized in Figs. 9c–9e. From the trajectory of the 1° step response (Fig. 9c), the closed-loop system is shown to have a 2% settling time T_s of 50 ms. As compared in Fig. 9d for a high walking speed (T_c =0.8 s), the measured $\theta_h(t)$ of the motorized hip joint closely tracks the reference $\alpha_h(t)$, and the mean absolute value of the tracking error is 1.7°, which is about 4.5% of the maximum value of the hip joint angle. Using Eq. (5) with the parametric values in Table 3, the needed torque and power of LEE for a specified healthy-leg trajectory $\theta_h(t)$ are simulated in Fig. 9e. The actuating torque (and hence power) is required only to overcome the small joint friction in the stance phase, and then increases rapidly (up to a maximum of 1.5 N·m) to lift the LEE against gravity in the swing phase.

3.2 Effects of P-BWS-LEE on internal knee force

BWS-LEE is designed to relieve the load on the injured knee during stance. As it is difficult (if not impossible) to measure the internal knee forces f_b, a published dynamic knee model (Lee and Wang, 2015; Wang DH et al., 2016) is used to simulate its effects. The knee model (Wang DH et al., 2016) is verified by comparing the simulated data with the sensor-embedded in-vivo data (Lee and Wang, 2015), and knee models from other researchers (Herzog and Read, 1993; Zheng et al., 1998; Kellis, 2001; Thambyah et al., 2005) are taken into account for reference. The average simulated knee forces and average measured plantar forces in MS and standing states from five gait trails (based on parametric data of five typical healthy subjects) are compared in Fig. 10 and Table 4, where

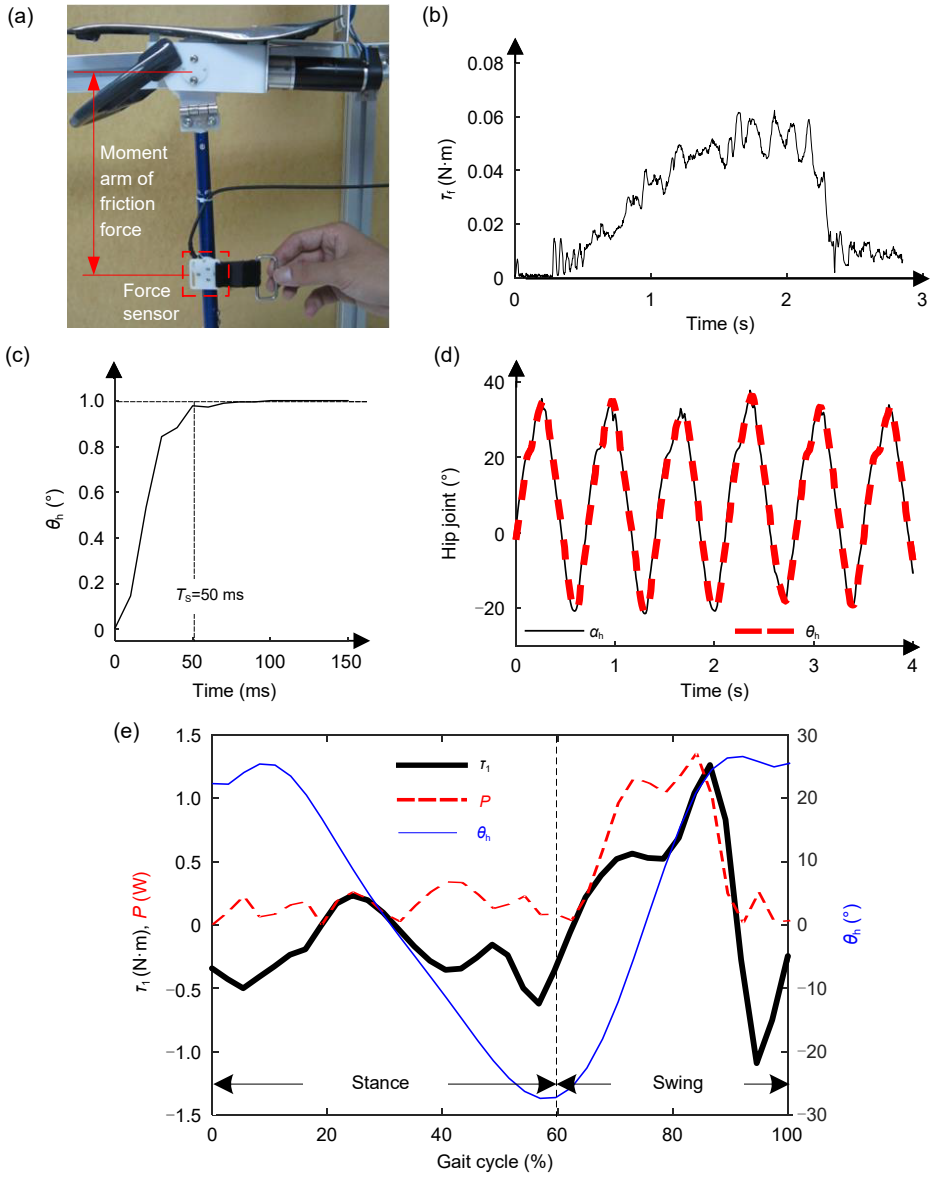

Fig. 9 Motor actuation system tests: (a) test platform; (b) low-friction torque in the motor-gear system; (c) step response; (d) real-time trajectory following; (e) dynamic simulation in LEE hip joint

the knee forces without LEE (C1) provide a basis for comparison. As demonstrated in Table 4, the plantar forces during standing still are reduced when wearing the LEE, verifying the contribution of the LEE in supporting the BW.

The reduced five-cycle knee forces in subject A (Fig. 10) show that the cyclical gaits have normally small fluctuations. However, for the five healthy subjects, in all cases, the passive LEE effectively reduces the mean plantar forces (12%–22%) and knee forces (13%–29%) in MS. The two peaks, which occur relatively consistently near the start and end of the MS, reveal a noticeable time delay caused by the passive LEE, which quantitatively increases the gait cycle time by 7%–78%, indicating that the subjects wearing the passive LEE walk slower and more conservatively than those without the LEE. Based on assessments after experiments, the testers report that the passive LEE loaded on their body restricts their joint flexion/extension and reduces their walking speed. It is expected that more familiarity and confidence over time are needed.

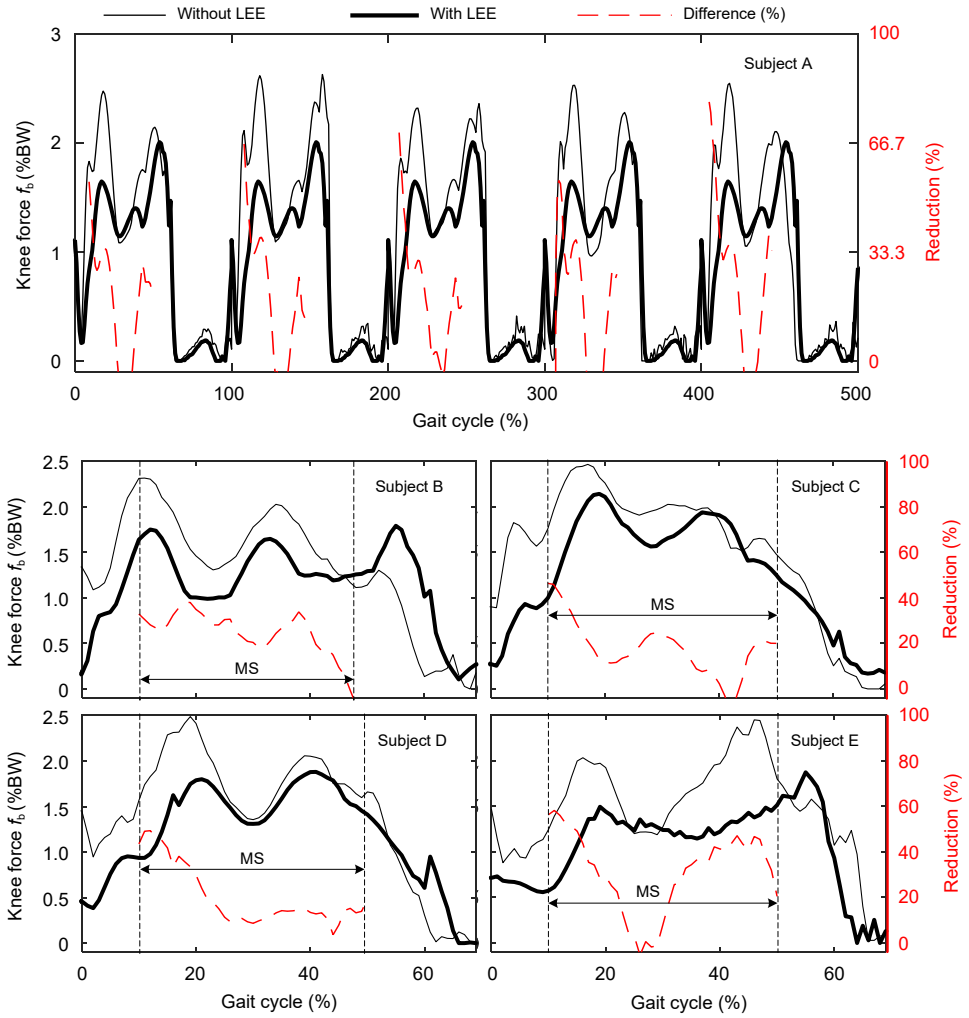

Fig. 10 Effect of gait cycle with and without passive LEE on knee force

Table 4 Simulated knee forces and measured plantar forces

Subject	Gender, age	Mass (kg)	Height (m)	Gate cycle (s)		Increase (%)
				No LEE	Passive LEE	
A	Male, 28	63.5	1.69	1.20	1.56	29.9
B	Male, 30	68.0	1.74	1.35	1.76	29.8
C	Male, 35	75.8	1.71	1.48	1.59	7.5
D	Female, 26	58.1	1.62	1.37	1.73	25.6
E	Male, 29	69.0	1.71	1.36	2.45	78.5

Subject	Plantar force in MS (%BM)		Reduction	Plantar force in standing (%BW)		Reduction	Knee force in MS (%BW)		Reduction
	No LEE	Passive LEE	(%)	No LEE	Passive LEE	(%)	No LEE	Passive LEE	(%)
A	0.87	0.67	22.2	0.5	0.404	19.2	1.71	1.36	20.7
B	0.92	0.78	15.8	0.5	0.411	17.8	1.65	1.32	19.9
C	0.93	0.82	12.2	0.5	0.414	17.2	1.96	1.69	13.6
D	0.95	0.83	12.4	0.5	0.403	19.4	1.85	1.53	17.0
E	0.94	0.80	14.9	0.5	0.416	16.8	1.76	1.23	29.9

Increase (%) represents the percentage of the increased gate cycle when wearing the LEE compared to the case with no LEE; reduction (%) represents the percentage of the reduced force when wearing the LEE compared to the case with no LEE. Both increase (%) and reduction (%) results are calculated using the raw data (without approximation)

3.3 Effect of the proposed LEE on gaits and weight compensation

Two sets of results for evaluating the LEE mechanism are presented. The first set (Fig. 11 and Table 5) is used to evaluate the gait synchronization of the injured leg/LEE with the healthy leg. The second set (Fig. 12) is used to evaluate the contribution of the motorized hip in relieving the BW on the potential injured knee during the swing phases.

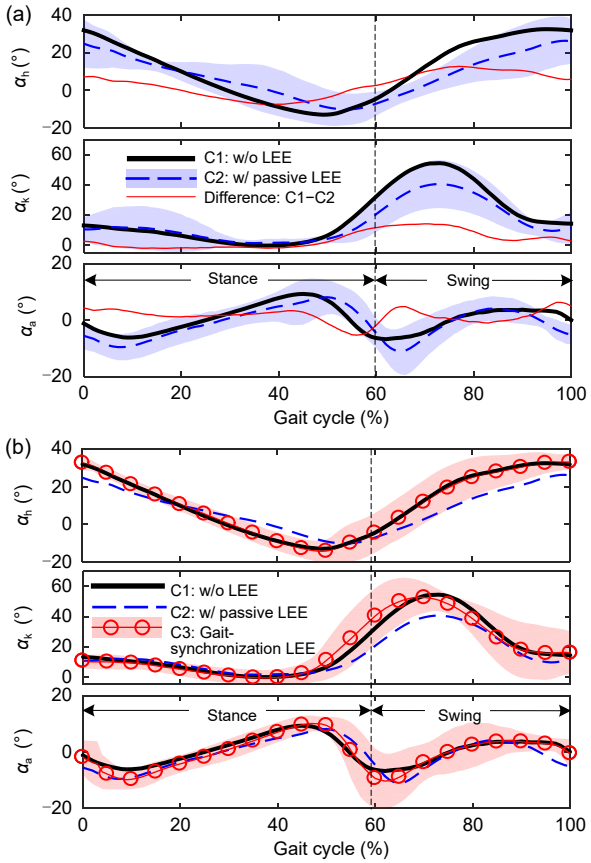

Fig. 11 Joint angle comparison with/without LEE: (a) joint angle difference with/without passive LEE; (b) joint angle difference with/without active hip LEE

3.3.1 Gait synchronization (1st set)

To evaluate gait synchronization, the left-leg sagittal joint angles are measured by three other IMUs (only for joint angle evaluation and not required in control, not shown in Fig. 3) while subject A (with both healthy legs but the left leg relying on BWS-LEE in experiments C2 and C3) walks 30 steps on a level floor. The results are summarized in Fig. 11 and Table 5. The abbreviations (C1, C2) and (C1, C3) denote that C2 and C3 are evaluated with respect to C1 in terms of four performance parameters, Ave, Max, *W*, and *D*, defined as follows:

1. Absolute (Ave, Max) differences of (C1, C2) and (C1, C3);

2. DTW alignment *W* defined in Eq. (A2) in Appendix;

3. Euler distance *D* between the two normalized sequences defined in Eq. (A4) in Appendix.

While (Ave, Max) give a snapshot comparison, *W* removes the effect of phase delay on gait synchronization before computing the absolute joint angle differences.

Fig. 11a graphs the joint angles for (C1, C2) in the sagittal plane as a basis for comparison, where the lines and the shaded envelopes display the average value and one standard deviation (of 30 steps), respectively. As compared in Fig. 11a, no significant joint angle differences are found between C2 and C1 during stance. However, some joint angle differences are noticeable during swing because of the lack of synchronization between the LEE and the leg; the weight/inertia of LEE tends to restrict the flexion of the hip and knee joints.

Fig. 11b compares the left hip joint angles of C1, C2, and C3. Unlike C2 where the LEE on the human leg restricts the hip/knee flexion and delays

Table 5 Comparisons of distances and angle differences

Term for comparison	Hip α_h	Knee α_k	Ankle α_a
Ave(C1, C2), Max(C1, C2) (°)	6.2, 12.7	5.0, 14.3	2.4, 6.3
Ave(C1, C3), Max(C1, C3) (°)	0.6, 1.5	2.6, 8.3	1.4, 3.7
Reduction of Ave(C1, C3) and Max(C1, C3) with respect to Ave(C1, C2) and Max(C1, C2), respectively (%)	90, 89	48, 42	44, 42
W(C1, C2), *W*(C1, C3) (°)	166.4, 28.1	220.6, 61.2	62.3, 58.9
Reduction of *W*(C1, C3) with respect to *W*(C1, C2) (%)	83	72	5
D(C1, C2), *D*(C1, C3) (°)	71.6, 7.4	68.4, 35.6	28.9, 17.5
Reduction of *D*(C1, C3) with respect to *D*(C1, C2) (%)	90	48	39

The values in % are calculated using the raw data (without approximation)

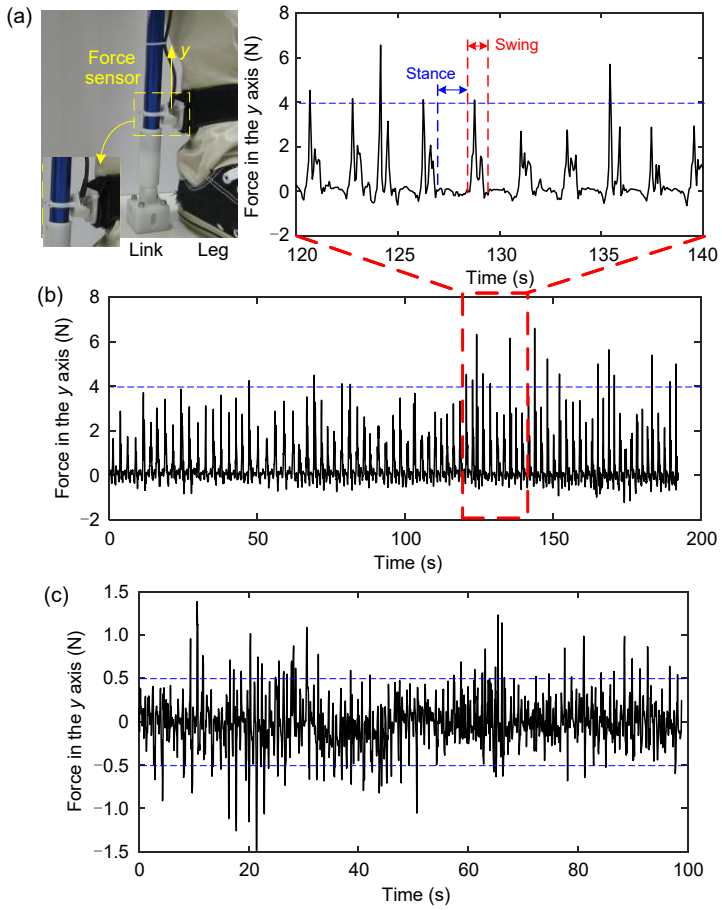

Fig. 12 Effect of passive LEE on joint angles and interaction force of subject A: (a) setup; (b) passive LEE; (c) motorized hip LEE

the ankle flexion, no significant differences in the joint angles of the hip, knee, and ankle between C1 and C3 are observed. As shown in Table 5, the absolute (Ave, Max) differences of the (hip, knee, ankle) angles between C1 and C3 are largely reduced compared with that between C1 and C2 by (90%, 48%, 44%) and (89%, 42%, 42%), respectively.

For quantitative comparison within a gait cycle, the DTW alignment W and Euler distance D of the unilateral LEE (C1, C3) with P-BWS-LEE (C1, C2) are calculated in Table 5, where the reductions in terms of percentage are computed relative to (C1, C2). Both the W_{hip}(C1, C3) and D_{hip}(C1, C3) values are lowered, by 83% and 90% respectively, demonstrating that the motorized hip joint plays an important role in gait synchronization of the injured leg. The W_{knee} and D_{knee} values are also reduced, by 72% and 48% respectively, indicating that the motorized hip design has a significant effect on synchronizing the knee joint. D_{ankle}(C1, C3) also decreases but the W_{ankle}(C1, C2) and W_{ankle}(C1, C3) values are similar and in the same order of magnitude, suggesting that the motorized hip design has negligible effects on the phase of the ankle angle.

3.3.2 Weight compensation (2nd set)

To determine the effects of P-BWS-LEE on the leg, the force sensor (ATI NANO17) is attached between the lower leg (above the ankle) and the end of the lower link (Fig. 12a). For simplicity, the footspring between the footpad (LEE) and shoe (human) is removed for measuring the dynamic force acting on the human leg due to LEE. Figs. 12b and 12c compare the forces measured along the y axis as subject A walks with C2 and C3, respectively.

As shown in Fig. 12b where the measured force on the leg with C2 is plotted, the load is transferred statically to the ground and hence there is no force

acting on the leg during stance, but it has a maximum value of about 4 N in each step during swing. This is because LEE loads its weight on the human foot, which restricts the knee flexion and causes a larger ankle dorsiflexion angle compared to the case with no LEE (C1). To synchronize LEE with the leg in the swing phases, more energy must be outputted to lift the links against gravity. With C3, the motorized hip joint helps LEE adapt to the human gait and minimize its loading effect on the gait during the swing phase; as a result, the measured (leg-LEE interaction) forces are of the order of 0.5 N or reduced by 87.5% from 4 N in C2.

4 Conclusions

A novel design of unilateral LEE has been proposed to help the one-side-knee-injured people walk normally. The LEE relieves the load on the injured leg by transferring the human BW directly to the ground during the stance phases while synchronizing its movements to follow the walking gait of the healthy leg to prevent hindering natural movements in the subsequent swing phase. The sensor-based method using a BWS-LEE with a motorized hip joint to synchronize a knee-injured leg with the healthy leg has been presented with training assessment.

The effectiveness of the proposed method has been evaluated experimentally on a prototype unilateral LEE. Average gait and time series data, which are compared between the BWS-LEE with and without the motorized hip joint, showed that gait synchronization significantly reduces the absolute average and maximum (hip, knee, ankle) angle differences between the healthy and injured legs by (90%, 48%, 44%) and (89%, 42%, 42%), respectively. With compact motorized hip joint that can be housed within a tight space under the seat, the measured (leg-LEE interaction) forces decreased by 87.5%, indicating that the motorized hip joint may relieve the loading effects on the injured gait during the swing phase. The mean plantar force decreased by 12%–22%, the simulated mean knee force decreased by 13%–29% accordingly, but the gait cycle increased by 7%–78%; these results indicated that the passive LEE has potential to support the BW in the stance phases and relieve the load on an injured knee, and that active LEE gait synchronization is necessary.

The exoskeleton training by natural gaits with and without LEE is only the first phase, and the preliminary results support the positive conclusions. The rigorous exoskeleton experimental methods include not only treadmill speed control, but also body parameter regression analysis, physiological evaluation, electromyography (EMG) signal measurement, and foot pressure distribution measurement. Because of the limited space in this paper, more exoskeleton scientific experiments are planned for publication in the future. While the unilateral LEE is illustrated in the context of an injured knee, it is expected that the proposed sensor-based method can be potentially extended to other LEE applications such as stroke rehabilitation where unilateral gait synchronization is essential.

Acknowledgements

The author thanks Drs. Kok-Meng LEE and Jingjing JI for technical advice and valuable discussion, and Luchen SHENG for assistance in experiments.

Compliance with ethics guidelines

Donghai WANG declares that he has no conflict of interest.

References

Barton G, Lisboa P, Lees A, et al., 2007. Gait quality assessment using self-organising artificial neural networks. *Gait Post*, 25(3):374-379. https://doi.org/10.1016/j.gaitpost.2006.05.003

Brophy R, Silvers HJ, Gonzales T, et al., 2010. Gender influences: the role of leg dominance in ACL injury among soccer players. *Br J Sports Med*, 44(10):694-697. https://doi.org/10.1136/bjsm.2008.051243

Chen B, Zhong CH, Zhao X, et al., 2019. Reference joint trajectories generation of CUHK-EXO exoskeleton for system balance in walking assistance. *IEEE Access*, 7:33809-33821. https://doi.org/10.1109/ACCESS.2019.2904296

Chen G, Qi P, Guo Z, et al., 2017. Gait-event-based synchronization method for gait rehabilitation robots via a bioinspired adaptive oscillator. *IEEE Trans Biomed Eng*, 64(6):1345-1356. https://doi.org/10.1109/TBME.2016.2604340

Dollar AM, Herr H, 2008. Lower extremity exoskeletons and active orthoses: challenges and state-of-the-art. *IEEE Trans Robot*, 24(1):144-158. https://doi.org/10.1109/TRO.2008.915453

Gupta R, Khanna T, Masih GD, et al., 2016. Acute anterior cruciate ligament injuries in multisport elite players: demography, association, and pattern in different sports. *J Clin Orthop Trauma*, 7(3):187-192.

https://doi.org/10.1016/j.jcot.2016.03.005

He Y, Li N, Wang C, et al., 2019. Development of a novel autonomous lower extremity exoskeleton robot for walking assistance. *Front Inform Technol Electron Eng*, 20(3): 318-329. https://doi.org/10.1631/FITEE.1800561

Herzog W, Read LJ, 1993. Lines of action and moment arms of the major force-carrying structures crossing the human knee joint. *J Anat*, 182(2):213-230. https://doi.org/10.1002/ar.1092350415

Hootman JM, Dick R, Agel J, 2007. Epidemiology of collegiate injuries for 15 sports: summary and recommendations for injury prevention initiatives. *J Athl Train*, 42(2): 311-319.

Kang I, Kunapuli P, Young AJ, 2020. Real-time neural network-based gait phase estimation using a robotic hip exoskeleton. *IEEE Trans Med Robot Bion*, 2(1):28-37. https://doi.org/10.1109/TMRB.2019.2961749

Kellis E, 2001. Tibiofemoral joint forces during maximal isokinetic eccentric and concentric efforts of the knee flexors. *Clin Biomech*, 16(3):229-236. https://doi.org/10.1016/s0268-0033(00)00084-x

Kim H, Shin YJ, Kim J, 2017. Design and locomotion control of a hydraulic lower extremity exoskeleton for mobility augmentation. *Mechatronics*, 46:32-45. https://doi.org/10.1016/j.mechatronics.2017.06.009

Lee KM, Wang DH, 2015. Design analysis of a passive weight-support lower-extremity-exoskeleton with compliant knee-joint. Proc IEEE Int Conf on Robotics and Automation, p.5572-5577. https://doi.org/10.1109/ICRA.2015.7139978

Li GY, Liu T, Yi JG, et al., 2016. The lower limbs kinematics analysis by wearable sensor shoes. *IEEE Sens J*, 16(8): 2627-2638. https://doi.org/10.1109/JSEN.2016.2515101

Li ZJ, Ren Z, Zhao KK, et al., 2020. Human-cooperative control design of a walking exoskeleton for body weight support. *IEEE Trans Ind Inform*, 16(5):2985-2996. https://doi.org/10.1109/TII.2019.2900121

Lin F, Wang AS, Zhuang Y, et al., 2016. Smart insole: a wearable sensor device for unobtrusive gait monitoring in daily life. *IEEE Trans Ind Inform*, 12(6):2281-2291. https://doi.org/10.1109/TII.2016.2585643

Liu Q, Qian GM, Meng W, et al., 2019. A new IMMU-based data glove for hand motion capture with optimized sensor layout. *Int J Intell Robot Appl*, 3:19-32. https://doi.org/10.1007/s41315-019-00085-4

Liu XH, Wang QN, 2020. Real-time locomotion mode recognition and assistive torque control for unilateral knee exoskeleton on different terrains. *IEEE/ASME Trans Mechatron*, 25(6):2722-2732. https://doi.org/10.1109/TMECH.2020.2990668

Long Y, Du ZJ, Wang WD, et al., 2018. Physical human-robot interaction estimation based control scheme for a hydraulically actuated exoskeleton designed for power amplification. *Front Inform Technol Electron Eng*, 19(9):1076-1085. https://doi.org/10.1631/FITEE.1601667

Lugade V, Lin V, Farley A, et al., 2014. An artificial neural network estimation of gait balance control in the elderly using clinical evaluations. *PLoS ONE*, 9(5):e97595. https://doi.org/10.1371/journal.pone.0097595

Malcolm P, Galle S, van den Berghe P, et al., 2018. Exoskeleton assistance symmetry matters: unilateral assistance reduces metabolic cost, but relatively less than bilateral assistance. *J Neuroeng Rehabil*, 15(1):74. https://doi.org/10.1186/s12984-018-0381-z

Mizukami N, Takeuchi S, Tetsuya M, et al., 2018. Effect of the synchronization-based control of a wearable robot having a non-exoskeletal structure on the hemiplegic gait of stroke patients. *IEEE Trans Neur Syst Rehabil Eng*, 26(5): 1011-1016. https://doi.org/10.1109/TNSRE.2018.2817647

Thambyah A, Pereira BP, Wyss U, 2005. Estimation of bone-on-bone contact forces in the tibiofemoral joint during walking. *Knee*, 12(5):383-388. https://doi.org/10.1016/j.knee.2004.12.005

Tsukahara A, Hasegawa Y, Eguchi K, et al., 2015. Restoration of gait for spinal cord injury patients using HAL with intention estimator for preferable swing speed. *IEEE Trans Neur Syst Rehabil Eng*, 23(2):308-318. https://doi.org/10.1109/TNSRE.2014.2364618

Uddin MZ, Hassan MM, Alsanad A, et al., 2020. A body sensor data fusion and deep recurrent neural network-based behavior recognition approach for robust healthcare. *Inform Fus*, 55:105-115. https://doi.org/10.1016/j.inffus.2019.08.004

Wang DH, Lee KM, Ji JJ, 2016. A passive gait-based weight-support lower extremity exoskeleton with compliant joints. *IEEE Trans Robot*, 32(4):933-942. https://doi.org/10.1109/TRO.2016.2572692

Wang TM, Pei X, Hou TG, et al., 2020. An untethered cable-driven ankle exoskeleton with plantarflexion-dorsiflexion bidirectional movement assistance. *Front Inform Technol Electron Eng*, 21(5):723-739. https://doi.org/10.1631/FITEE.1900455

Wang ZL, Zhao HY, Qiu S, et al., 2015. Stance-phase detection for ZUPT-aided foot-mounted pedestrian navigation system. *IEEE Trans Mechatron*, 20(6):3170-3181. https://doi.org/10.1109/TMECH.2015.2430357

Yu H, Wang DH, Yang CJ, et al., 2010. A walking monitoring shoe system for simultaneous plantar-force measurement and gait-phase detection. Proc IEEE/ASME Int Conf on Advanced Intelligent Mechatronics, p.207-212. https://doi.org/10.1109/AIM.2010.5695868

Zhang C, Liu GF, Li CL, et al., 2016. Development of a lower limb rehabilitation exoskeleton based on real-time gait detection and gait tracking. *Adv Mech Eng*, 8(1):1-9. https://doi.org/10.1177/1687814015627982

Zhang T, Tran M, Huang H, 2018. Design and experimental verification of hip exoskeleton with balance capacities for walking assistance. *IEEE/ASME Trans Mechatron*, 23(1): 274-285. https://doi.org/10.1109/TMECH.2018.2790358

Zheng NQ, Fleisig GS, Escamilla RF, et al., 1998. An analytical model of the knee for estimation of internal forces during exercise. *J Biomech*, 31(10):963-967. https://doi.org/10.1016/S0021-9290(98)00056-6

Appendix: Dynamic-time-warping method

The dynamic-time-warping (DTW) method is used to evaluate the similarity between two joint trajectories (of different lengths):

$$\boldsymbol{x}=\left(x_1, x_2, \cdots, x_m\right),\ \boldsymbol{y}=\left(y_1, y_2, \cdots, y_n\right).$$

The optimal alignment p between them is found using the DTW method minimizing a cost function $\boldsymbol{C}$ with element

$$C_{ij}=\left|x_i-y_j\right|, i=1,2,...,m, j=1,2,...,n. \quad \text{(A1)}$$

Intuitively, p runs along a "valley of low cost" within the cost matrix $\boldsymbol{C}$. Thus, the optimal alignment is also a warping path having a minimum total cost among all possible warping paths defined in Eqs. (A2) and (A3), where the subscript ℓ indicates an element along the warping path with length L in $\boldsymbol{C}$:

$$W(\boldsymbol{x},\boldsymbol{y})=\min\left\{c_p(\boldsymbol{x},\boldsymbol{y})\,\middle|\, p \text{ is an } (m,n) \text{ alignment}\right\}, \quad \text{(A2)}$$

where

$$c_p(\boldsymbol{x},\boldsymbol{y})=\sum_{\ell=1}^{L} C_{i_\ell j_\ell}. \quad \text{(A3)}$$

In Eq. (A3), $C_{i_\ell j_\ell}$ is the element chosen from each row of the cost matrix $\boldsymbol{C}$ such that the chosen L elements are connected to form a warping path. Once two similar sequences are aligned, they are then normalized to the same length (m=n) for similarity evaluation using the Euler distance D between these two normalized sequences as defined in Eq. (A4):

$$D=\sqrt{\sum_{i=1}^{n}(x_i-y_i)^2}. \quad \text{(A4)}$$